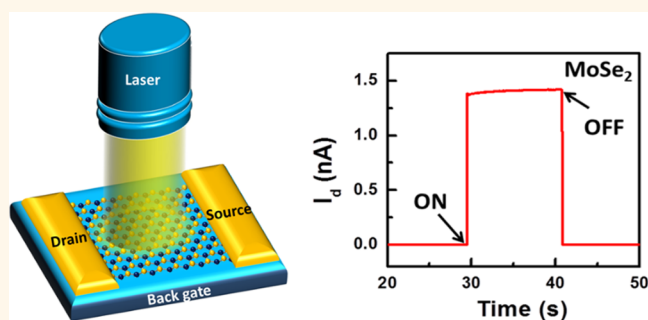


Monolayer MoSe₂ Grown by Chemical Vapor Deposition for Fast Photodetection

Yung-Huang Chang,^{†,○} Wenjing Zhang,^{‡,§,○} Yihan Zhu,[‡] Yu Han,[‡] Jiang Pu,^{||} Jan-Kai Chang,[†] Wei-Ting Hsu,[#] Jing-Kai Huang,[†] Chang-Lung Hsu,[†] Ming-Hui Chiu,[‡] Taishi Takenobu,^{||,△} Henan Li,[▼] Chih-I Wu,[†] Wen-Hao Chang,[#] Andrew Thye Shen Wee,[‡] and Lain-Jong Li^{†,‡,*}

[†]Institute of Atomic and Molecular Sciences, Academia Sinica, Taipei 11529, Taiwan, [‡]Department of Physics, National University of Singapore, 117542 Singapore, [§]SZU-NUS Collaborative Innovation Center for Optoelectronic Science & Technology, Key Laboratory of Optoelectronic Devices and Systems of Ministry of Education, Guangdong Province, Shenzhen University, Shenzhen 518060, China, ^{||}Physical Science and Engineering Division, King Abdullah University of Science and Technology, Thuwal 23955-6900, Saudi Arabia, ^{||}Department of Advanced Science and Engineering, Waseda University, Tokyo 169-8555, Japan, [#]Institute of Photonics and Optoelectronics and Department of Electrical Engineering, National Taiwan University, Taipei 10617, Taiwan, [△]Department of Electrophysics, National Chiao Tung University, Hsinchu 30010, Taiwan, [△]Department of Applied Physics, Kagami Memorial Laboratory for Material Science and Technology, Waseda University, Tokyo 169-8555, Japan, and [▼]School of Materials Science and Engineering, Nanyang Technological University, 639798 Singapore. [○]These authors contributed equally.

ABSTRACT Monolayer molybdenum disulfide (MoS₂) has become a promising building block in optoelectronics for its high photosensitivity. However, sulfur vacancies and other defects significantly affect the electrical and optoelectronic properties of monolayer MoS₂ devices. Here, highly crystalline molybdenum diselenide (MoSe₂) monolayers have been successfully synthesized by the chemical vapor deposition (CVD) method. Low-temperature photoluminescence comparison for MoS₂ and MoSe₂ monolayers reveals that the MoSe₂ monolayer shows a much weaker bound exciton peak; hence, the phototransistor based on MoSe₂ presents a much faster response time (<25 ms) than the corresponding 30 s for the CVD MoS₂ monolayer at room temperature in ambient conditions. The images obtained from transmission electron microscopy indicate that the MoSe exhibits fewer defects than MoS₂. This work provides the fundamental understanding for the differences in optoelectronic behaviors between MoSe₂ and MoS₂ and is useful for guiding future designs in 2D material-based optoelectronic devices.



KEYWORDS: transition metal dichalcogenides · photoresponse · MoSe₂ · MoS₂ · two-dimensional materials

Transition metal dichalcogenides (TMDs) with the formula MX₂, where M is a transition metal (Mo, W, and so on) and X is a chalcogen (S, Se, or Te), have attracted much attention due to their layer structure and semiconducting properties.^{1–6} These two-dimensional (2D) materials are in the form of X–M–X, where a plane of metal atoms is sandwiched between two planes of chalcogen atoms by covalent interaction, and different layers are held together by van der Waals interactions.^{7,8} These layer materials exhibit many distinctive characteristics such as outstanding flexibility,⁹ moderate carrier mobility,^{10,11} and layer-dependent electronic and optical properties.^{12–20} Thus, the TMD materials can serve as transparent and flexible field-effect transistors (FETs),^{21–24} photodetectors,²⁵

photovoltaic cells,^{26,27} light-emitting diodes,^{28,29} and catalysts.^{30–32} In particular, TMD materials have been reported to absorb up to 5–10% of incident sunlight within a thickness less than 1 nm, which is about 1 order of magnitude higher absorption than GaAs and Si.²⁶ The phototransistors based on monolayer MoS₂ show outstanding photoresponsivity even up to a few thousand A/W.^{25,33} Recently, a graphene/MoS₂ hybrid phototransistor was demonstrated to be able to provide a photogain of more than 10⁸.³⁴ However, the long response time of 4–30 s for monolayer MoS₂-based phototransistors, caused by persistent photocarriers generated from trapped defects or charged impurity states,^{25,33,34} limits their application for fast photon detection.

* Address correspondence to lance.sinica@gmail.com.

Received for review June 17, 2014 and accepted August 5, 2014.

Published online August 05, 2014
10.1021/nn503287m

© 2014 American Chemical Society

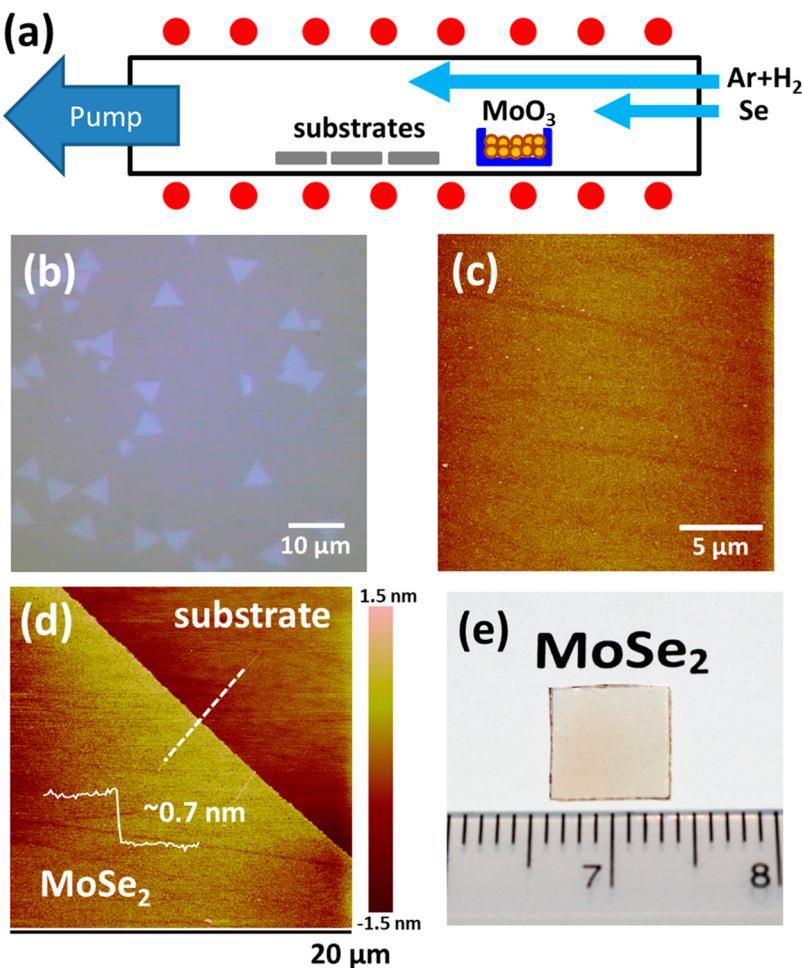


Figure 1. (a) Schematic illustration for the growth of MoSe₂ layers on sapphire substrates by the selenization of MoO₃ powders in a CVD furnace. (b) OM. (c) AFM image of the monolayer MoSe₂ flakes and monolayer film grown at 800 °C, where the difference is the location of the substrates in the furnace. (d) AFM image and (e) OM of a monolayer MoSe₂ film grown at 800 °C on a sapphire substrate.

Recently, monolayer MoSe₂ has started to gain attention because it has many interesting electronic and optical properties similar to those of monolayer MoS₂, such as a direct band gap, strong photoluminescence (PL), and a large exciton binding energy.^{35–41} It is known that sulfur defects in the MoS₂ monolayer greatly affect the electronic transport and optical properties. Therefore, it would be meaningful to carefully compare the properties of monolayer MoS₂ and MoSe₂. One important question is whether the MoSe₂ monolayer grown by chemical vapor deposition (CVD) exhibits better optoelectronic characteristics. In this study, we synthesized monolayer MoSe₂ on sapphire by the gas phase reaction between MoO₃ and Se powders in a hot-wall tube furnace system, using a CVD method which has been reported elsewhere.^{4,6} X-ray photoemission spectroscopy (XPS) and transmission electron microscopy (TEM) measurements confirm that the MoSe₂ film is highly crystalline. By comparing the electrical devices fabricated with these two monolayers, we demonstrate that both MoS₂ and MoSe₂ monolayers exhibit a comparable mobility

value for the electron transport. It is also noteworthy that electrical and ultraviolet photoemission spectroscopy (UPS) measurements demonstrate that MoS₂ is heavily n-doped but MoSe₂ is less n-doped. Low-temperature photoluminescence study reveals that the MoSe₂ monolayer has a much weaker bound exciton peak, indirectly suggesting that the MoSe₂ monolayer possesses fewer defects or impurities. Most interestingly, the CVD MoSe₂ monolayer exhibits a much faster response time (<25 ms) than MoS₂, making it superior for fast photodetection applications.

RESULTS AND DISCUSSION

Synthesis of the MoSe₂ Monolayer. The experimental setup for growing monolayer MoSe₂ using MoO₃ and Se powder precursors in a hot-wall CVD system is schematically illustrated in Figure 1a. Hydrogen was introduced as a reducing agent during the growth process.⁵ The morphology of the MoSe₂ grown on sapphire substrates varies with the distance of the substrate from the MoO₃ source, as shown in Figures 1b,c. The optical micrograph (OM) in Figure 1b shows that

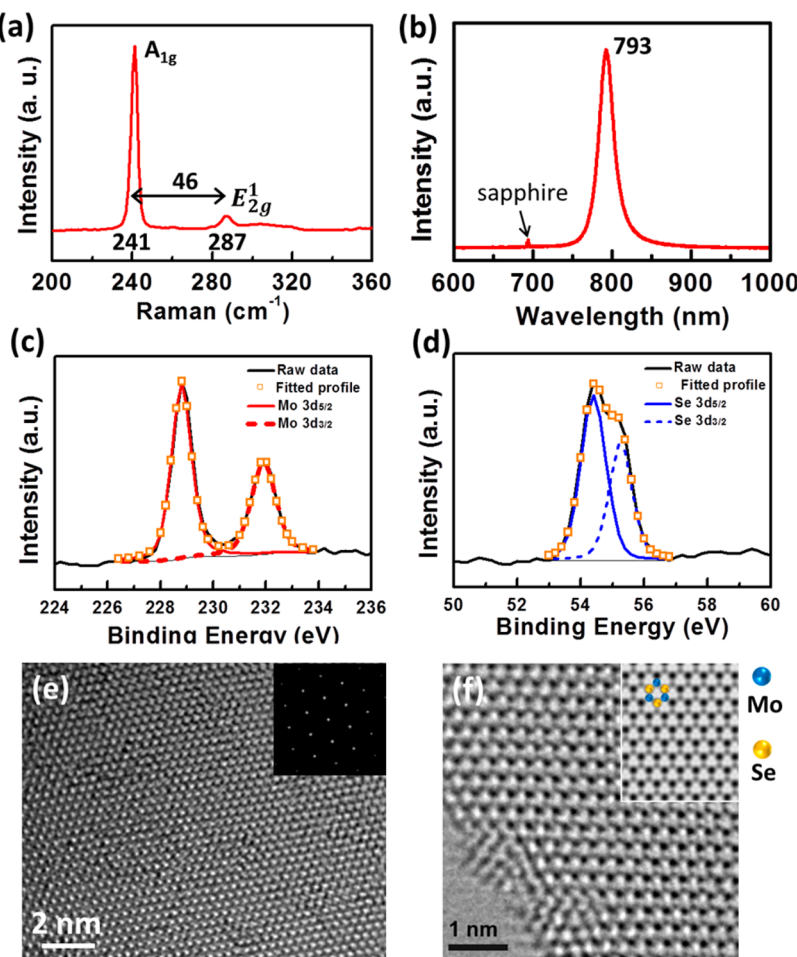


Figure 2. (a) Raman spectrum for the monolayer MoSe_2 , obtained in a confocal Raman spectrometer excited by a 473 nm laser. (b) Photoluminescence spectra for the CVD monolayer MoSe_2 , obtained in a microscopic PL system (excitation wavelength 532 nm). (c,d) XPS spectra of the monolayer MoSe_2 film, where the (c) Mo 3d and (d) Se 3d binding energies are identified. (e) High-resolution TEM image of monolayer MoSe_2 with an inset showing its Fourier transform pattern. (f) Enlarged TEM image, where the Mo and Se atoms are identified. The inset is a simulated HRTEM image of monolayer MoSe_2 .

the sparsely distributed triangular crystals (lateral size $\sim 5 \mu\text{m}$) are found in most areas of the substrate located furthest from the MoO_3 source. When the substrate is close to the MoO_3 source, the nucleation density becomes much higher such that these small domains easily merge to form a continuous film, as shown in the atomic force microscopy (AFM) image in Figure 1c. Moreover, the cross-sectional height profile in Figure 1d shows that the thickness of the MoSe_2 film is $\sim 0.7 \text{ nm}$, corresponding to a monolayer and consistent with published monolayer thickness.^{6,37} Figure 1e shows the OM of the MoSe_2 monolayer. In addition to the MoSe_2 monolayer, we occasionally observe the growth of second-layer MoSe_2 on top of some monolayer flakes, as shown in Supporting Information Figure S1. The occasionally found MoSe_2 second layers are normally in the areas with high substrate roughness or with some particles, likely due to the rough surfaces or particles that are able to assist the nucleation of the second layer.

Structural Characterization of MoSe_2 . The layer dependence of Raman features has been reported for TMDs

such as MoS_2 , MoSe_2 , and WSe_2 .^{7,16,38,40} In Figure 2a, the synthesized monolayer MoSe_2 exhibits two characteristic peaks located at 241.2 and 286.7 cm^{-1} , associated with the out-of-plane A_{1g} mode and in-plane E_{2g}^1 mode, respectively.^{6,35} Furthermore, the Raman peak at $\sim 353 \text{ cm}^{-1}$, which has been demonstrated to relate to the interlayer interaction, is not observed in our monolayer MoSe_2 .³⁸ This suggests that the CVD synthesized MoSe_2 is indeed one monolayer. Figure 2b displays the PL spectrum for monolayer MoSe_2 . Only a strong peak located at 793 nm is observed, attributed to the direct band gap emission from A excitons.^{6,35,37} It is noted that the indirect gap emission is absent in the monolayer, and the strong A exciton emission from the monolayer is in good agreement with a recent report.^{38,41} In addition, the XPS spectra for the CVD synthesized monolayer MoSe_2 in Figure 2c,d confirm the stoichiometry of MoSe_2 . The peaks at 228.8 and 232 eV are attributed to the doublet $\text{Mo } 3d_{5/2}$ and $\text{Mo } 3d_{3/2}$ binding energies, respectively, for Mo^{4+} .^{42,43} The peaks corresponding to the $\text{Se } 3d_{5/2}$ and $\text{Se } 3d_{3/2}$ orbitals of

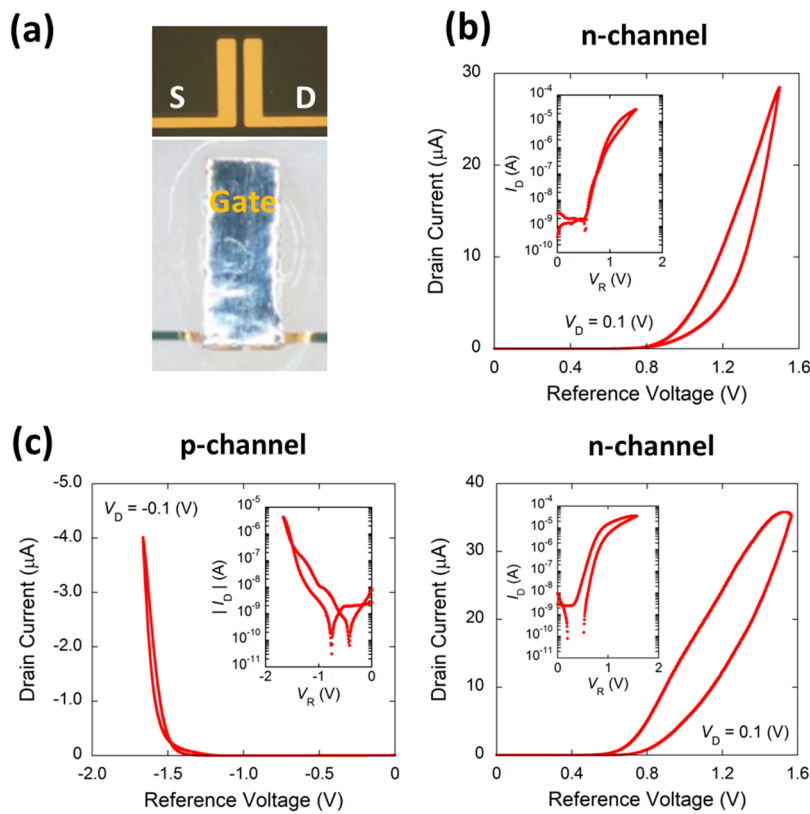


Figure 3. (a) Optical micrograph (top view) for the MoSe₂ EDLT device, where the top and bottom photos were taken before and after the ion gel/top-gate deposition. (b,c) Typical transfer curves of the (b) MoS₂ and (c) MoSe₂ EDLT devices, where the inset in each graph shows the transfer curve plotted in a log scale.

divalent selenide ions (Se²⁻) are observed at 54.4 and 55.2 eV.^{42,43} Aberration-corrected high-resolution TEM (HRTEM) images demonstrate a high crystallinity of monolayer MoSe₂, in which the Se and Mo atomic columns can be directly identified (Figure 2e,f). The remarkable contrast difference between Se and Mo is in good agreement with the simulated HRTEM image for monolayer MoSe₂ (Figure 2f). The lattice constant of the 2D hexagonal lattice is measured directly from the image and the corresponding Fourier transform and determined to be $a = 0.323$ nm, consistent with that of bulk MoSe₂.

Electric Double-Layer Transistors. The electrical characteristics of the electric double-layer transistors (EDLTs) were measured directly for the monolayer MoSe₂ films on sapphire substrates. The detailed description of EDLT fabrication was reported in previous studies^{3,5} and is illustrated in Figure S2. The output characteristics for the MoSe₂ devices are also shown in Figure S2. Figure 3a shows the OM top view image of the MoSe₂ EDLT, where the channel width and length are 90 and 1000 μ m, respectively. Figure 3c displays the p- and n-channel drain current as a function of the reference voltage V_R for monolayer MoSe₂ EDLT at the applied drain voltage V_D = -0.1 and 0.1 V, respectively. Note that V_R is the measured voltage between the electrolytes and MoSe₂, that is, the voltage for the electric

double layer on MoSe₂ surfaces. Since the gate voltage applied on the top Pt metal is partially consumed by the electric double layer on the gate electrode, V_R is used instead for the gate dependence measurements. Although some reports have claimed that MoSe₂ is an n-type semiconductor,⁴⁴ we clearly observe an ambipolar transport behavior instead since the electric double layer exhibits a higher gating efficiency. Figure 3c shows that the threshold voltage for the n-channel is 0.64 V in the forward scan, smaller than the 1.46 V value for the p-channel, indicating that the MoSe₂ is an n-type preferred ambipolar semiconductor. However, a unipolar n-type electrical characteristic is presented for MoS₂ using the same EDLT technology as shown in Figure 3b. Furthermore, we did not observe any hole transport current in the same negative gate voltage range (-1.6 to 0 V) for MoS₂. The field-effect mobility was calculated using the standard formula in the linear region, $\mu = (L/WC_iV_D) \times (\Delta I_D/\Delta V_R)$, where μ is the field-effect mobility, W is the channel width, V_D is the drain voltage, C_i is the measured specific capacitance of the ion gel, L is the channel length, and I_D is the drain current. The highest carrier mobility obtained for the MoSe₂ monolayer is 23 cm²/Vs for electron transport and 15 cm²/Vs for hole transport. For the MoS₂ monolayer, the electron mobility is around 17 cm²/Vs. As shown in the insets of

Figure 3b–d, the current ON–OFF ratio is as high as 10^4 – 10^5 for both MoSe₂ and MoS₂. The comparative EDLT measurement results for both MoSe₂ and MoS₂ are listed in Table 1. In brief, MoSe₂ exhibits a similar electron mobility value and ON–OFF current ratio compared with MoS₂, which also makes it a promising candidate for FET applications.

Ultraviolet Photoemission Spectroscopy. UPS is used to explore the energy level alignment with respect to the Fermi energy (E_F). The MoS₂ and MoSe₂ monolayers are separately transferred onto Si substrates coated with 60 nm thermally evaporated Au. The Au layer serves as a reference for E_F , assigned to 0 eV.^{45,46} As shown in Figure 4a, the valence band (E_V) for MoS₂ and MoSe₂ on Au/Si substrates is, respectively, located at 1.75 and 1.20 eV below E_F by linearly extrapolating the leading edge of the spectrum to the baseline. In addition, the work function (Φ) can be calculated using $\Phi = h\nu - E_{\text{onset}}$, where $h\nu$ is the incident photon energy (40.8 eV)

TABLE 1. Summarization of the MoS₂ and MoSe₂ from EDLT Measurements

mobility (cm ² /Vs)				
hole	electron	ON/OFF	type	
MoS ₂	~17	10^4 – 10^5	n-type	
MoSe ₂	~15	10^4 – 10^5	ambipolar	

^aThe n-type preferred.

and E_{onset} is the onset level related to the secondary electrons, as shown in Figure 4b.⁴⁷ Hence, the Φ for MoS₂ and MoSe₂ on Au/Si substrates is 4.20 and 4.27 eV, respectively. Note that the work function value obtained for monolayer MoS₂ is consistent with several other reports.^{48–51} In addition, the optical band gaps of the CVD monolayer MoS₂ and MoSe₂ are determined to be \sim 1.83 and \sim 1.51 eV, respectively, from the absorption spectra (Figure S3). Thus, the energy band diagrams of CVD monolayer MoS₂ and MoSe₂ relative to the Fermi level E_F of gold films are illustrated in Figure 4c,d. The energy separation ΔE between the conduction band of MoS₂ and the E_F of Au is \sim 0.08 eV, indicating that CVD monolayer MoS₂ is heavily n-doped, consistent with unipolar n-type electrical transport behavior. On the other hand, the energy separation ΔE between the conduction band of MoSe₂ and the E_F of Au is \sim 0.31 eV, indicating that the CVD monolayer MoSe₂ is slightly n-doped, consistent with the n-type preferred ambipolar electrical transport behavior.

Optical Properties. To examine the gate-dependent photoresponse characteristics, the MoS₂ and the MoSe₂ films are transferred onto 300 nm SiO₂/Si substrates, and the phototransistors are patterned using standard photolithography. Figure S4 shows the optical image of the interdigitated electrodes used, where the contact metal layers, 10 nm Ti and 80 nm Au, are deposited by thermal evaporation. The 532 and

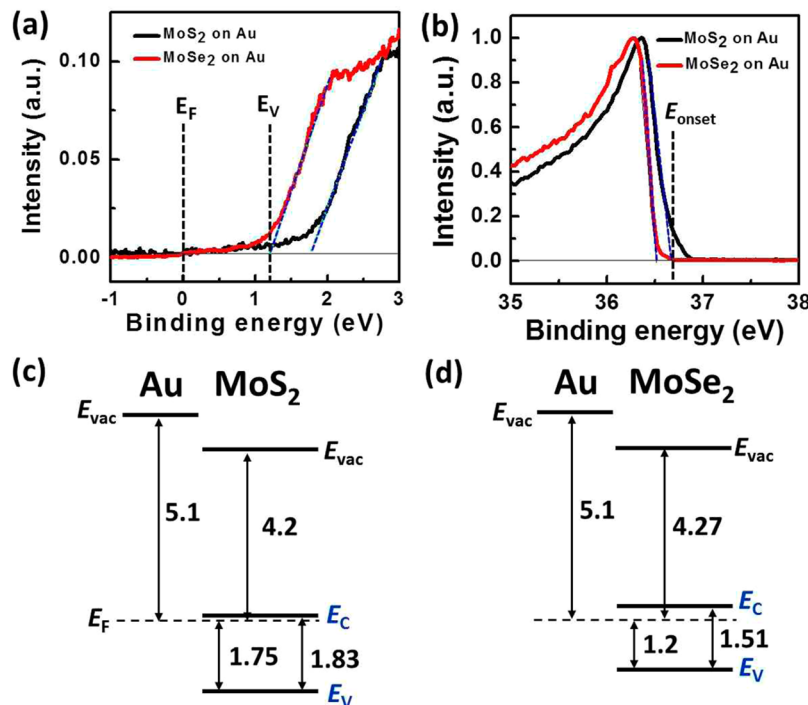


Figure 4. Ultraviolet photoemission spectroscopy and energy band diagrams. (a) UPS spectra, near the Fermi level energy and valence band maximum, of the monolayer MoS₂ and MoSe₂ film transferred onto the 60 nm Au-coated Si substrates. (b) Onset level (E_{onset}) of the UPS spectra, where the work function (Φ) can be calculated by $\Phi = h\nu - E_{\text{onset}}$, $h\nu$ is the incident photon energy of 40.8 eV. (c,d) Energy band diagrams of the monolayer (c) MoS₂ and (d) MoSe₂ film, where Au metal is used as a reference. Note that the band gap energies used in diagram are optical gaps.

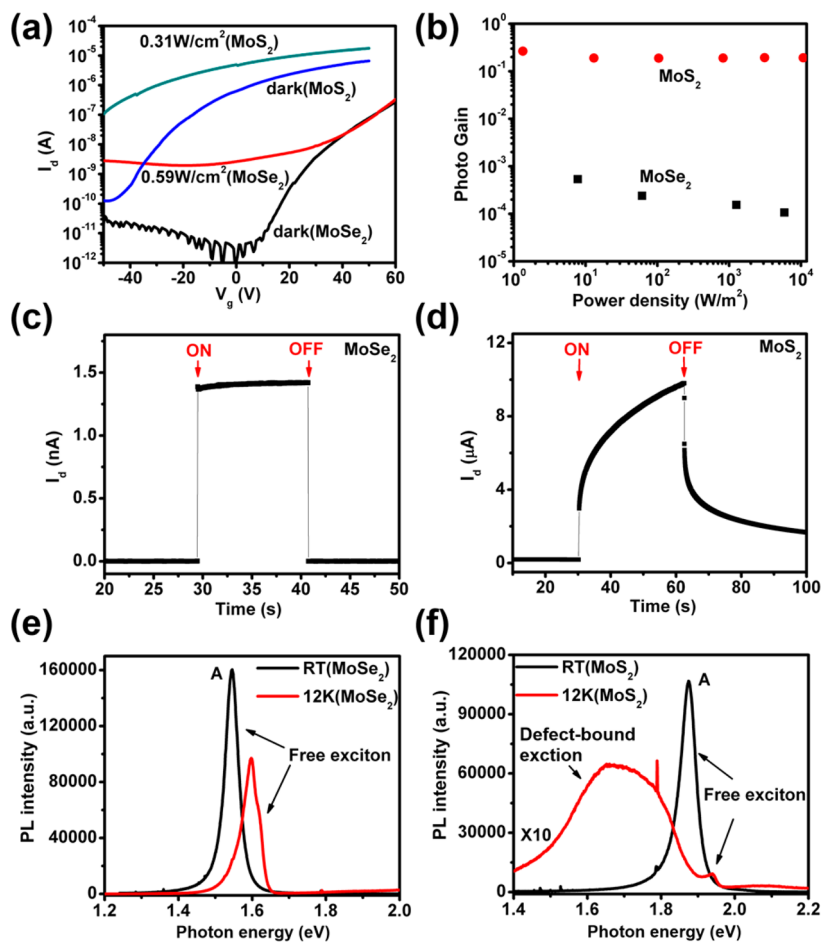


Figure 5. Optical properties of CVD MoSe₂ and MoS₂ monolayers. (a) I_d – V_g transfer characteristics of the photodetectors based on CVD MoSe₂ and MoS₂ monolayers in dark and under illumination at $V_{ds} = 1$ V. (b) Power density dependence of the photogain at $V_{ds} = 1$ V for the photodetectors at the OFF state, where V_g is 0 V for the MoSe₂ and V_g is –48 V for the MoS₂. (c,d) Time-resolved photocurrents of the photodetectors based on MoSe₂ at $P = 0.59$ W/cm² and MoS₂ at $P = 0.31$ W/cm². (e,f) PL spectra of monolayer MoSe₂ and MoS₂, respectively, at room temperature (RT) and 12 K.

650 nm CW lasers are used as the light sources to study the MoS₂ and MoSe₂ phototransistors. Figure 5a presents the typical transport curves of the two phototransistors in the dark and under illumination. In the dark, the n-channel subthreshold voltage V_{th} of the MoSe₂ and MoS₂ is ~7 V and ~–46 V, respectively, corroborating that the MoS₂ on SiO₂ is much more heavily n-doped. The mobilities of MoSe₂ and MoS₂ transistors are ~0.012 cm²/Vs at $V_g = 60$ V ($V_g - V_{th} = 53$ V) and ~0.021 cm²/Vs at $V_g = 17$ V ($V_g - V_{th} = 53$ V), respectively. Compared with the devices on sapphire, the mobilities of the devices on SiO₂ are about 3 orders of magnitude lower, which may be caused by several factors including the possible degradation by transfer processes, the scattering effect from charge impurities added during the transfer process, and damage caused by patterning. Under illumination at a power density of ~0.31 and 0.59 W/cm², the OFF state currents of both devices increase by ~3 orders of magnitude. The photogain (G), given by $G = h\nu I_{ph}/(\eta e P_0)$,³³ is an index to quantify the conversion efficiency of incident photons to photogenerated carriers, where I_{ph} is the

net photocurrent, P_0 is the absorbed laser power, h is Planck's constant, e is the charge of an electron, and ν is the frequency of incident light. Assuming $\eta = 100\%$, the photogain of the MoS₂ phototransistors is ~0.2, much higher than ~5 × 10^{–4} of the MoSe₂ phototransistor in the OFF state. The MoSe₂ band diagrams in Figure 4c,d indicate that the electron Schottky barrier of MoSe₂ is higher,⁵² resulting in the smaller photogain of MoSe₂ on SiO₂. This also accounts for the lower OFF state dark current for MoSe₂ (~10^{–12} A vs ~10^{–10} A for MoS₂).

Figure 5c,d shows the time-resolved photocurrent for monolayer MoSe₂ and MoS₂ films, respectively, under ON/OFF light illumination at $V_{ds} = 1$ V in ambient environment. A fast rise and decay response time shorter than ~25 ms for MoSe₂ is observed. However, the photocurrent of the MoS₂ phototransistors takes more than 30 s to saturate and decay. The persistent photocurrent is normally attributed to defect or charge impurity states inside the band gap.⁵³ Figure 5e,f shows the PL spectra of the monolayer MoSe₂ and MoS₂ at room and low temperatures. We observe only

one peak at room temperature, ~ 1.55 eV for the MoSe_2 and ~ 1.88 eV for the MoS_2 , corresponding to the direct band-to-band A excitonic transition. The peak intensity for monolayer MoSe_2 at room temperature is stronger than that of monolayer MoS_2 , and the full width at half-maximum of ~ 42 meV for monolayer MoSe_2 is smaller than the ~ 51 meV value of monolayer MoS_2 . When the temperature decreases to 12 K, an additional sub-band-gap emission at the low energy side between 1.4 and 1.9 eV appears for the monolayer CVD MoS_2 , which could be attributed to the defect or charge impurity states.^{15,53} Due to the additional binding to defects or charge impurities, the energy of the bound exciton peak is lower than that of the free exciton peak.¹⁵ The large width of the bound exciton peak indicates the presence of different kinds of defects or charge impurity sites since different binding energies are needed. In contrast, no sub-band-gap emission is observed at the low-energy side for the CVD MoSe_2 monolayer, implying better crystalline quality and fewer defects or charge impurity states, thus resulting in higher band-to-band free exciton recombination rates. Some reports have pointed out that the persistent photoconductance arises from the defects or charge impurity states inside the band gap.^{33,54,55} Hence, the extra photogenerated carriers in the MoS_2 arising from the defects or charge impurity states could be responsible for its slow light response time. Figure S5 shows the HRTEM image for the CVD MoS_2 monolayers with

abundantly disordered atom arrangement highlighted by dashed circles, which is in clear contrast to the HRTEM for CVD MoSe_2 in Figure 2e,f.

Moreover, the CVD MoS_2 shows significantly lower stability in ambient environment, where its PL intensity normally decays in 2 or 3 days. We notice that the shelf-lifetime can be increased to more than 1 week if the sample is stored in a drybox, indicating that the moisture may react or catalyze the formation of defects in MoS_2 . By contrast, PL measurements suggest that the CVD MoSe_2 monolayer exhibits a much longer shelf-lifetime, typically more than 4 weeks, in the same ambient storage condition. These observations are also in line with a relatively larger amount of defects in MoS_2 revealed by TEM.

CONCLUSIONS

In conclusion, we have synthesized crystalline monolayer MoSe_2 by the gas phase selenization of MoO_3 in a hot-wall CVD chamber. From the analyses of EDLT and UPS measurements, the MoSe_2 exhibits a slight n-type preferred ambipolar behavior, while the MoS_2 shows heavily n-doped electrical characteristics. In addition, the defect-less crystalline structure for the MoSe_2 is identified through the low-temperature PL, whereas relatively abundant defects occur in MoS_2 . This study shows that CVD synthesized monolayer MoSe_2 has great potential in flexible transparent optoelectronic applications.

METHODS

Growth of MoSe_2 Monolayers. The MoO_3 powders (0.025–0.3 g) were placed in a ceramic boat located in the heating zone center of the furnace. The Se powders were placed in a separate quartz boat at the upper stream side maintained at 270 °C during the reaction. The sapphire substrates for growing MoSe_2 were placed at the downstream side near MoO_3 powders, where the Se and MoO_3 vapors were brought to the targeting sapphire substrates by an Ar/H_2 flowing gas ($\text{Ar} = 40$ –70 sccm, $\text{H}_2 = 10$ sccm, chamber pressure = 25–350 Torr). The center heating zone was heated to 700–900 °C at a ramp rate 15 °C/min. After the growth temperature was reached, the heating zone was kept for 15 min and the furnace was then naturally cooled to room temperature.

Fabrication of EDLT Devices. For the source and drain electrodes, Au contacts with Ni adhesion layers (70 nm/2 nm) were thermally deposited onto the surface of the MoSe_2 films. The ion gels, a mixture of a triblock copolymer, poly(styrene-block-methyl methacrylate-block-styrene) (PS-PMMA-PS; MPS = 4.3 kg/mol, MPMMA = 12.5 kg/mol, M_w = 21.1 kg/mol), and an ionic liquid, 1-ethyl-3-methylimidazoliumbis(trifluoromethylsulfonyl)imide ([EMIM][TFSI]) in an ethyl propionate solution, were used as the top-gate dielectrics. Note that the weight ratio of the polymer, ionic liquid, and solvent was maintained at 0.7:9.3:20. This solution was drop-casted onto and covered the surfaces of MoSe_2 film and the source and drain electrodes. The transistor channel was then covered with a thin Pt foil (thickness of 0.03 mm) to form the top-gate electrode. Finally, a thin gold wire was inserted into the gel films, between the channel and top-gate metal, as the reference electrode. All electrical characterizations were performed using a semiconductor parameter analyzer (Agilent E5270) in a shield probe station inside a N_2 -filled glovebox.

Characterizations. Photoluminescence spectra were excited by a green light laser with 532 nm wavelength and a 0.9 NA objective (spot size: 0.7 μm). Raman spectra were collected in a NT-MDT confocal Raman microscopic system (laser wavelength = 473 nm and laser spot size ~ 0.5 μm). The Si peak at 520 cm^{-1} was used as reference for wavenumber calibration. The AFM images were performed in a Veeco Dimension-Icon system. Chemical configurations were determined by X-ray photoelectron spectroscopy (Phi V5000). XPS measurements were performed with an Mg K α X-ray source on the samples. The energy calibrations were made against the C 1s peak to eliminate the charging of the sample during analysis. The valence band UPS were performed using He I (21.2 eV) and He II (40.8 eV) photon lines as excitation sources, and the photoelectrons were analyzed with a hemispherical analyzer with an overall resolution of 0.05 eV. The absorbance spectra were obtained using a JASCO-V-670 UV-vis spectrophotometer. The MoSe_2 films were transferred onto a copper grid for TEM observation. HRTEM imaging was performed on an aberration-corrected and monochromated G² cubed Titan 60-300 electron microscope under 60 kV. The electrical measurements were performed using a Keithley semiconductor parameter analyzer, model 4200-SCS. All the measurements were achieved at room temperature in ambient air. Continuous wavelength 532 and 650 nm lasers were used to measure the photoresponse of the devices, and the spot size was ~ 1 mm.

Conflict of Interest: The authors declare no competing financial interest.

Acknowledgment. This research was supported by Academia Sinica, National Science Council Taiwan (102-2119-M-001-005) and AFOSR-BRI USA. T.T. was partially supported by the

Funding Program for the Next Generation of World-Leading Researchers and Grants-in-Aid from MEXT (26107533 "Science of Atomic Layers" and 25000003 "Specially Promoted Research").

Supporting Information Available: Raman spectra are included. This material is available free of charge via the Internet at <http://pubs.acs.org>.

REFERENCES AND NOTES

- Chhowalla, M.; Shin, H. S.; Eda, G.; Li, L.-J.; Loh, K. P.; Zhang, H. The Chemistry of Two-Dimensional Layered Transition Metal Dichalcogenide Nanosheets. *Nat. Chem.* **2013**, *5*, 263–275.
- Wang, Q. H.; Kalantar-Zadeh, K.; Kis, A.; Coleman, J. N.; Strano, M. S. Electronics and Optoelectronics of Two-Dimensional Transition Metal Dichalcogenides. *Nat. Nanotechnol.* **2012**, *7*, 699–712.
- Lee, Y. H.; Zhang, X. Q.; Zhang, W.; Chang, M. T.; Lin, C. T.; Chang, K. D.; Yu, Y.-C.; Wang, T. W.; Chang, C.-S.; Li, L. J.; et al. Synthesis of Large-Area MoS₂ Atomic Layers with Chemical Vapor Deposition. *Adv. Mater.* **2012**, *24*, 2320–2325.
- Lee, Y.-H.; Yu, L.; Wang, H.; Fang, W.; Ling, X.; Shi, Y.; Lin, C.-T.; Huang, J.-K.; Chang, M.-T.; Chang, C.-S.; et al. Synthesis and Transfer of Single Layer Transition Metal Disulfides on Diverse Surfaces. *Nano Lett.* **2013**, *13*, 1852–1857.
- Huang, J.-K.; Pu, J.; Hsu, C.-L.; Chiu, M.-H.; Juang, Z.-Y.; Chang, Y.-H.; Chang, W.-H.; Iwasa, Y.; Takenobu, T.; Li, L.-J. Large-Area Synthesis of Highly Crystalline WSe₂ Monolayers and Device Applications. *ACS Nano* **2014**, *8*, 923–930.
- Shaw, J. C.; Zhou, H.; Chen, Y.; Weiss, N. O.; Liu, Y.; Huang, Y.; Duan, X. Chemical Vapor Deposition Growth of Monolayer MoSe₂ Nanosheets. *Nano Res.* **2014**, *7*, 1–7.
- Huang, X.; Zeng, Z.; Zhang, H. Metal Dichalcogenide Nanosheets: Preparation, Properties and Applications. *Chem. Soc. Rev.* **2013**, *42*, 1934–1946.
- Ataca, C.; Sahin, H.; Ciraci, S. Stable, Single-Layer MX₂ Transition-Metal Oxides and Dichalcogenides in a Honeycomb-like Structure. *J. Phys. Chem. C* **2012**, *116*, 8983–8999.
- Pu, J.; Yomogida, Y.; Liu, K.-K.; Li, L.-J.; Iwasa, Y.; Takenobu, T. Highly Flexible MoS₂ Thin-Film Transistors with Ion Gel Dielectrics. *Nano Lett.* **2012**, *12*, 4013–4017.
- Radisavljevic, B.; Radenovic, A.; Brivio, J.; Giacometti, V.; Kis, A. Single-Layer MoS₂ Transistors. *Nat. Nanotechnol.* **2011**, *6*, 147–150.
- Radisavljevic, B.; Whitwick, M. B.; Kis, A. Integrated Circuits and Logic Operations Based on Single-Layer MoS₂. *ACS Nano* **2011**, *5*, 9934–9938.
- Splendiani, A.; Sun, L.; Zhang, Y.; Li, T.; Kim, J.; Chim, C.-Y.; Galli, G.; Wang, F. Emerging Photoluminescence in Monolayer MoS₂. *Nano Lett.* **2010**, *10*, 1271–1275.
- Mak, K. F.; Lee, C.; Hone, J.; Shan, J.; Heinz, T. F. Atomically Thin MoS₂: A New Direct-Gap Semiconductor. *Phys. Rev. Lett.* **2010**, *105*, 136805.
- Lee, C.; Yan, H.; Brus, L. E.; Heinz, T. F.; Hone, J.; Ryu, S. Anomalous Lattice Vibrations of Single- and Few-Layer MoS₂. *ACS Nano* **2010**, *4*, 2695–2700.
- Korn, T.; Heydrich, S.; Hirmer, M.; Schmutzler, J.; Schüller, C. Low-Temperature Photocarrier Dynamics in Monolayer MoS₂. *Appl. Phys. Lett.* **2011**, *99*, 102109.
- Ghatak, S.; Pal, A. N.; Ghosh, A. Nature of Electronic States in Atomically Thin MoS₂ Field-Effect Transistors. *ACS Nano* **2011**, *5*, 7707–7712.
- Eda, G.; Yamaguchi, H.; Voiry, D.; Fujita, T.; Chen, M.; Chhowalla, M. Photoluminescence from Chemically Exfoliated MoS₂. *Nano Lett.* **2011**, *11*, 5111–5116.
- Zeng, H.; Dai, J.; Yao, W.; Xiao, D.; Cui, X. Valley Polarization in MoS₂ Monolayers by Optical Pumping. *Nat. Nanotechnol.* **2012**, *7*, 490–493.
- Mak, K. F.; He, K.; Shan, J.; Heinz, T. F. Control of Valley Polarization in Monolayer MoS₂ by Optical Helicity. *Nat. Nanotechnol.* **2012**, *7*, 494–498.
- Mak, K. F.; He, K.; Lee, C.; Lee, G. H.; Hone, J.; Heinz, T. F.; Shan, J. Tightly Bound Triions in Monolayer MoS₂. *Nat. Mater.* **2013**, *12*, 207–211.
- Kashid, R. V.; Late, D. J.; Chou, S. S.; Huang, Y.-K.; De, M.; Joag, D. S.; More, M. A.; Dravid, V. P. Enhanced Field-Emission Behavior of Layered MoS₂ Sheets. *Small* **2013**, *9*, 2730–2734.
- Kim, S.; Konar, A.; Hwang, W.-S.; Lee, J. H.; Lee, J.; Yang, J.; Jung, C.; Kim, H.; Yoo, J.-B.; Choi, J.-Y.; et al. High-Mobility and Low-Power Thin-Film Transistors Based on Multilayer MoS₂ Crystals. *Nat. Commun.* **2012**, *3*, 1011.
- Yu, W. J.; Li, Z.; Zhou, H.; Chen, Y.; Wang, Y.; Huang, Y.; Duan, X. Vertically Stacked Multi-heterostructures of Layered Materials for Logic Transistors and Complementary Inverters. *Nat. Mater.* **2013**, *12*, 246–252.
- Lin, J. D.; Zhong, J. Q.; Zhong, S.; Li, H.; Zhang, H. Modulating Electronic Transport Properties of MoS₂ Field Effect Transistor by Surface Overlays. *Appl. Phys. Lett.* **2013**, *103*, 063109.
- Lopez-Sanchez, O.; Lembke, D.; Kayci, M.; Radenovic, A.; Kis, A. Ultrasensitive Photodetectors Based on Monolayer MoS₂. *Nat. Nanotechnol.* **2013**, *8*, 497–501.
- Bernardi, M.; Palummo, M.; Grossman, J. C. Extraordinary Sunlight Absorption and One Nanometer Thick Photovoltaics Using Two-Dimensional Monolayer Materials. *Nano Lett.* **2013**, *13*, 3664–3670.
- Fontana, M.; Deppe, T.; Boyd, A. K.; Rinzan, M.; Liu, A. Y.; Paranjape, M.; Barbara, P. Electron–Hole Transport and Photovoltaic Effect in Gated MoS₂ Schottky Junctions. *Sci. Rep.* **2013**, *3*, 1634.
- Britnell, L.; Ribeiro, R. M.; Eckmann, A.; Jalil, R.; Belle, B. D.; Mishchenko, A.; Kim, Y.-J.; Gorbachev, R. V.; Georgiou, T.; Morozov, S. V.; et al. Strong Light–Matter Interactions in Heterostructures of Atomically Thin Films. *Science* **2013**, *340*, 1311–1314.
- Ross, J. S.; Klement, P.; Jones, A. M.; Ghimire, N. J.; Yan, J.; Mandrus, D. G.; Taniguchi, T.; Watanabe, K.; Kitamura, K.; Yao, W.; et al. Electrically Tunable Excitonic Light-Emitting Diodes Based on Monolayer WSe₂ p–n Junctions. *Nat. Nanotechnol.* **2014**, *9*, 268–272.
- Chang, Y.-H.; Lin, C.-T.; Chen, T.-Y.; Hsu, C.-L.; Lee, Y.-H.; Zhang, W.; Wei, K.-H.; Li, L.-J. Highly Efficient Electrocatalytic Hydrogen Production by MoS_x Grown on Graphene-Protected 3D Ni Foams. *Adv. Mater.* **2013**, *25*, 756–760.
- Chang, Y.-H.; Wu, F.-Y.; Chen, T.-Y.; Hsu, C.-L.; Chen, C.-H.; Wiryo, F.; Wei, K.-H.; Chiang, C.-Y.; Li, L.-J. Three-Dimensional Molybdenum Sulfide Sponges for Electrocatalytic Water Splitting. *Small* **2014**, *10*, 895–900.
- Xiang, Q.; Yu, J.; Jaroniec, M. Synergistic Effect of MoS₂ and Graphene as Cocatalysts for Enhanced Photocatalytic H₂ Production Activity of TiO₂ Nanoparticles. *J. Am. Chem. Soc.* **2012**, *134*, 6575–6578.
- Zhang, W.; Huang, J.-K.; Chen, C.-H.; Chang, Y.-H.; Cheng, Y.-J.; Li, L.-J. High-Gain Phototransistors Based on a CVD MoS₂ Monolayer. *Adv. Mater.* **2013**, *25*, 3456–3461.
- Zhang, W.; Chuu, C.-P.; Huang, J.-K.; Chen, C.-H.; Tsai, M.-L.; Chang, Y.-H.; Liang, C.-T.; Chen, Y.-Z.; Chueh, Y.-L.; He, J.-H.; et al. Ultrahigh-Gain Photodetectors Based on Atomically Thin Graphene–MoS₂ Heterostructures. *Sci. Rep.* **2014**, *4*, 3826.
- Tongay, S.; Zhou, J.; Ataca, C.; Lo, K.; Matthews, T. S.; Li, J.; Grossman, J. C.; Wu, J. Thermally Driven Crossover from Indirect toward Direct Bandgap in 2D Semiconductors: MoSe₂ versus MoS₂. *Nano Lett.* **2012**, *12*, 5576–5580.
- Horzum, S.; Sahin, H.; Cahangirov, S.; Cudazzo, P.; Rubio, A.; Serin, T.; Peeters, F. M. Phonon Softening and Direct to Indirect Band Gap Crossover in Strained Single-Layer MoSe₂. *Phys. Rev. B* **2013**, *87*, 125415.
- Ross, J. S.; Wu, S.; Yu, H.; Ghimire, N. J.; Jones, A. M.; Aivazian, G.; Yan, J.; Mandrus, D. G.; Xiao, D.; Yao, W.; et al. Electrical Control of Neutral and Charged Excitons in a Monolayer Semiconductor. *Nat. Commun.* **2013**, *4*, 1474.
- Tonndorf, P.; Schmidt, R.; Böttger, P.; Zhang, X.; Börner, J.; Liebig, A.; Albrecht, M.; Kloc, C.; Gordan, O.; Zahn, D. R. T.; et al. Photoluminescence Emission and Raman Response of Monolayer MoS₂, MoSe₂, and WSe₂. *Opt. Express* **2013**, *21*, 4908–4916.

39. Kang, J.; Tongay, S.; Zhou, J.; Li, J.; Wu, J. Band Offsets and Heterostructures of Two-Dimensional Semiconductors. *Appl. Phys. Lett.* **2013**, *102*, 012111.

40. Lee, C.; Yan, H.; Brus, L. E.; Heinz, T. F.; Hone, J.; Ryu, S. Anomalous Lattice Vibrations of Singleand Few-Layer MoS₂. *ACS Nano* **2011**, *5*, 2695–2700.

41. Zeng, H.; Liu, G.-B.; Dai, J.; Yan, Y.; Zhu, B.; He, R.; Xie, L.; Xu, S.; Chen, X.; Yao, W.; *et al.* Optical Signature of Symmetry Variations and Spin-Valley Coupling in Atomically Thin Tungsten Dichalcogenides. *Sci. Rep.* **2013**, *3*, 1608.

42. Abdallah, W. A.; Nelson, A. E. Characterization of MoSe₂-(0001) and Ion-Sputtered MoSe₂ by XPS. *J. Mater. Sci.* **2005**, *40*, 2679–2681.

43. Pouzet, J.; Berneude, J. C. MoSe₂ Thin Films Synthesized by Solid State Reactions between Mo and Se Thin Films. *Rev. Phys. Appl.* **1990**, *25*, 807–815.

44. Larentis, S.; Fallahazad, B.; Tutuc, E. Field-Effect Transistors and Intrinsic Mobility in Ultra-thin MoSe₂ Layers. *Appl. Phys. Lett.* **2012**, *101*, 223104.

45. Wu, C. I.; Kahn, A. Investigation of the Chemistry and Electronic Properties of Metal/Gallium Nitride Interfaces. *J. Vac. Sci. Technol., B* **1998**, *16*, 2218–2223.

46. Chen, M. H.; Wu, C. I. Roles of Thermally Evaporated Cesium Oxide in Organic Light Emitting Diodes. *J. Appl. Phys.* **2008**, *104*, 113713.

47. Chen, C.-Y.; Retamal, J. R. D.; Wu, I.-W.; Lien, D.-H.; Chen, M. W.; Ding, Y.; Chueh, Y.-L.; Wu, C.-I.; He, J.-H. Probing Surface Band Bending of Surface-Engineered Metal Oxide Nanowires. *ACS Nano* **2012**, *6*, 9366–9372.

48. Schlaf, R.; Lang, O.; Pettenkofer, C.; Jaegermann, W. Band Lineup of Layered Semiconductor Heterointerfaces Prepared by van der Waals Epitaxy: Charge Transfer Correction Term for the Electron Affinity Rule. *J. Appl. Phys.* **1999**, *85*, 2732–2753.

49. Choi, M. S.; Lee, G.-H.; Yu, Y.-J.; Lee, D.-Y.; Lee, S. H.; Kim, P.; Hone, J.; Yoo, W. J. Controlled Charge Trapping by Molybdenum Disulphide and Graphene in Ultrathin Heterostructured Memory Devices. *Nat. Commun.* **2013**, *4*, 1624.

50. Fu, D.; Zhou, J.; Tongay, S.; Liu, K.; Fan, W.; Liu, T.-J. K.; Wu, J. Mechanically Modulated Tunneling Resistance in Monolayer MoS₂. *Appl. Phys. Lett.* **2013**, *103*, 183105.

51. Kang, J.; Tongay, S.; Zhou, J.; Li, J.; Wu, J. Band Offsets and Heterostructures of Two-Dimensional Semiconductors. *Appl. Phys. Lett.* **2013**, *102*, 012111.

52. Yin, Z.; Li, H.; Li, H.; Jiang, L.; Shi, Y.; Sun, Y.; Lu, G.; Zhang, Q.; Chen, X.; Zhang, H. Single-Layer MoS₂ Phototransistors. *ACS Nano* **2012**, *6*, 74–80.

53. Tongay, S.; Suh, J.; Ataca, C.; Fan, W.; Luce, A.; Kang, J. S.; Liu, J.; Ko, C.; Raghunathan, R.; Zhou, J.; *et al.* Defects Activated Photoluminescence in Two-Dimensional Semiconductors: Interplay between Bound, Charged, and Free Excitons. *Sci. Rep.* **2013**, *3*, 2657.

54. Zhang, A.; You, S.; Soci, C.; Liu, Y.; Wang, D.; Lo, Y.-H. Silicon Nanowire Detectors Showing Phototransistive Gain. *Appl. Phys. Lett.* **2008**, *93*, 121110.

55. Lany, S.; Zunger, A. Anion Vacancies as a Source of Persistent Photoconductivity in II–VI and Chalcopyrite Semiconductors. *Phys. Rev. B* **2005**, *72*, 035215.